Sodium pumps adapt spike bursting to stimulus statistics

Sara Arganda[1,2 *], Raúl Guantes[3*], Gonzalo G. de Polavieja[1,2 #]

[1]Neural Processing Laboratory, Instituto 'Nicolás Cabrera' de Física de Materiales, Universidad Autónoma de Madrid, 28049 Spain
[2]Department of Theoretical Physics, Universidad Autónoma de Madrid
[3]Department of Condensed Matter Physics, Universidad Autónoma de Madrid

[*] Equally contributing authors
[#] To whom correspondence should be addressed. E-mail: gonzalo.polavieja@uam.es

KEY WORDS: sodium-potassium ATPase, neural coding, variance, mechanoreception
Running head: Pumps adapt bursting to statistics
Abstract: 147 words
Main text: 3895 words
Contains 6 color figures
Supplementary information in separate file

Pump activity is a homeostatic mechanism maintaining ionic gradients. Here we test whether the slow reduction in excitability induced by sodium pump activity seen in many neuronal types can also play a role in neuronal coding. We record intracellularly from a spike bursting sensory neuron in response to naturalistic stimulation using different statistical distributions. We show that the regulation of excitability by sodium pumps is necessary for the neuron to respond differently depending on the statistical context of stimuli. In particular, sodium pump activity allows spike burst sizes and rates to code not for stimulus values *per se* but their ratio with the standard deviation of the stimulus distribution. Modeling further shows that sodium pumps can be a general mechanism of adaptation to statistics in the time scale of a minute. These results implicate the ubiquitous pump activity in the adaptation to statistics in neural codes.

Adaptation to static stimuli is a well-known phenomenon in nervous systems. To understand function and mechanisms responsible for the flexibility of neuronal systems under real-world changes, it is however necessary to study adaptation to stimuli in their statistical context. Adaptation to the stimulus mean, the simplest parameter of a distribution, is a basic processing strategy in all sensory modalities that allows sensitivity to fluctuations around the mean[1,2]. A more sophisticated strategy is the adaptation to the variance of the stimulus distribution[3-9] and perhaps to higher-order moments[10]. Stimulus variance also changes in time in natural conditions and adapting to it allows matching output range to input range and a higher information transfer[7,8,11].

Despite the fundamental role of adaptation to stimulus variance for the correct functioning of many systems, the underlying mechanisms remain largely unknown. Theoretical analysis and experimental evidence argue in favor of the existence of multiple mechanisms probably to span several time scales and to work under different constraints[12-20]. At the single neuron level, current injection experiments have implicated slow sodium inactivation in bipolar cells[18,21] and sodium-dependent potassium conductances in cortex[20].

The sodium-potassium ATPase, or sodium pump, is ubiquitous in neurons. During firing, Na^+ ions accumulate inside the axon, driving the sodium pump that continues its activity even when the spike trains have ceased. The sodium pump exchanges three internal Na^+ ions for two external K^+ ions and the resulting imbalance recovers the membrane from depolarization and can even hyperpolarize the membrane. The membrane hyperpolarization reduces membrane excitability, for example in dopaminergic neurons[22], spinal networks[23], hippocampus[24,25], C-fibers in bullfrog sciatic nerve[26], insect mechanoreceptors[27] and human skin receptors[28].

We reasoned that the ability of the sodium pump to control excitability could in principle be a single-neuron mechanism for adaptation to stimulus variance. While the faster dynamics of ion

channels allows neurons to respond to particular stimulus features, the slow hyperpolarizing dynamics of sodium pumps effectively integrates past firing activity and affects future firing. Sodium pump activity may then allow neurons to respond to stimulus features relative to the stimulus statistics. To test this hypothesis in a functionally relevant setting, we have turned to spiking receptors, a preparation that allows naturalistic stimulation and minimizes the interference from synaptic and network effects. We use as our experimental system the skin deformation receptor neuron in the leech *Hirudo medicinalis* known as T (tactile) neuron. The spike receptor T neuron used to test this hypothesis responds to simple step stimuli on the skin with spike bursts. The advantage of this receptor neuron is that sodium pump is known to control its excitability in the scale of a minute[29-36], allowing for a clean test of our hypothesis that sodium pump activity can adapt neuronal codes to stimulus statistics. In response to a train of action potentials, sodium pump activity induces in this neuron a hyperpolarization of up to approximately 30 mV and lasting a minute. Another hyperpolarizing current acting in this neuron is the calcium-dependent potassium current, but has a lower amplitude of up to 5 mV[30,37].

To study adaptation to stimulus variance we first need to determine the neuronal code. This is particularly interesting in our case since the neuron responds in bursts of spikes, thought to be a distinct mode of communication in sensory systems[38]. Bursts facilitate synaptic transmission, can improve the signal-to-noise ratio of responses and detect certain signals better than isolated spikes[38,39]. Another important issue in burst coding is which are the burst parameters relevant for information transmission. Several proposals have given, including spike frequency[40], burst duration[41,42] and latency of the first spike[43].

Here we have undertaken the study of the possible role of the sodium pump as a mechanism for adaptation to stimulus variance and its relevance for a burst code. The paper is organized as

follows. First, we show that the sodium pump hyperpolarizes more the membrane for higher stimulus velocity variance. This hyperpolarization has the effect of decreasing excitability with increasing stimulus velocity variance. Second, we show that the neuron codes stimulus velocity into burst sizes and burst rates. Third, we show that the hyperpolarization induced by sodium pump activity has an important impact on the code. The neuron codes in bursts sizes and burst rates not the stimulus velocity *per se* but velocity scaled by the standard deviation of the stimulus velocity distribution. This adaptive scaling is found to be significantly disrupted in presence of the sodium pump blocker strophantidin. On the other hand, blocking the calcium-dependent potassium current with apamin has no significant effect on adaptational scaling. A model of the receptor neuron further shows that sodium pumps alone can explain the observed adaptation to stimulus variance in the scale of a minute.

RESULTS

Sodium pump-induced reduction in membrane excitability increases with stimulus variance

The sodium pump is responsible in the receptor neuron for adaptation in a slow time scale, (**Fig. 1a**). The effect of the sodium pump in adaptation was first seen using a simple protocol of skin stimulation, consisting of small 40 μm steps at a frequency of 1.5Hz before and after 20s of skin displacements following several sinusoidal patterns of amplitude 400 μm at 10Hz (**Fig. 1a, bottom**). During the sinusoidal stimulation the membrane hyperpolarizes 10mV and does not respond to the following step stimuli for 20s (**Fig. 1a, top**), except when we bath the preparation with strophantidin (**Fig. 1a, middle**), a well-known blocker of the sodium pump[30,31]. The hyperpolarization induced by the pump activity after firing thus increases the voltage to spike threshold.

We next studied how the hyperpolarization and reduction in firing depend on the stimulus variance (**Fig. 1b-f**). It is illustrative to consider the raw spikes produced when the neuron is already adapted. The skin was stimulated with one of two gaussian white-noise distributions of displacements with different standard deviations, σ =0.0425 mm (in velocity σ_{vel} =0.75 mm/s) or 0.1275 mm (2.25 mm/s), (**Fig. 1b**, red and blue lines, respectively). The neuron responds with spike bursts preferentially to slope in stimulus position (stimulus velocity) as in the case of simple displacement step stimuli to which it responds only at stimulus onset and offset (**Figure S1a**). More surprising is the similarity in the firing characteristics for the two stimulus distributions despite their large difference in variance. This is possible because for larger input velocity variance the neuron is more hyperpolarized (23mV and 27mV for σ_{vel} =0.75 and σ_{vel} =2.25 mm/s, respectively) and therefore in a state of reduced excitability. For the same value of input velocity there is then less response when the input distribution has larger velocity variance.

We then quantified the dependence of hyperpolarization and reduction of excitability with stimulus variance, (**Fig. 1c-f**). The hyperpolarization ΔV increases with increasing stimulus velocity standard deviation up to a value of 28 mV at σ_{vel} =3.25 mm/s (**Fig. 1c**). Reduction of excitability with increasing σ_{vel} is also apparent in the spiking rate obtained in the following manner. We calculated the initial average firing rate r_{av} for the first second of stimulation as a function of the velocity standard deviation σ_{vel} (**Fig. 1d**). The initial rate is higher with increasing σ_{vel} until a value of around 40 spikes/s at σ_{vel} =3.25 mm/s (**Fig. 1d**, black points). We then calculate the average firing rate when the neuron is adapted after 10 min of stimulation. This rate is smaller and depends less on the velocity standard deviation, reaching a value of 13 spikes/s for σ_{vel} >2.25 mm/s (**Fig. 1d**, white squares). The reduction of excitability can then be calculated as the difference

between the spike rate at the beginning and when the neuron is adapted, r_{av} (t=1s)- r_{av} (t=10 min), that increases with velocity standard deviation and varies in the interval 0-27 spikes/s. Neither hyperpolarization values nor reduction in excitability were found to depend significantly on the value of cut-off frequency used in the stimulus (5, 10 and 20 Hz in **Fig. 1**), but only on stimulus velocity standard deviation.

The dynamics of adaptation is of the order a minute for the range of the stimulus cut-off frequencies 5-20 Hz considered (**Fig. 1e,f**). At the start of stimulation, the firing rate r_{av} is higher for larger standard deviation of stimulus velocities, illustrated here for two gaussian distributions with cut-off frequency of 5Hz and σ_{vel}=0.75 mm/s (red) or 2.25 mm/s (blue) (**Fig. 1f)**. Spiking activity in turn activates the sodium pump and the membrane hyperpolarizes by values ΔV, larger for the higher spike rates, that is, for larger stimulus velocity variance (**Fig. 1e**). Hyperpolarization in turn reduces excitability as seen in the decay of spike rates in time, (**Fig. 1f)**. For the first 10s there is an abrupt decay in the average spike rate and a slower decay for approximately a minute until stationary firing is reached.

Burst size and rate code for mechanical velocity

To find how the sodium pump-induced hyperpolarization affects the coding properties, we first determined which code the neuron uses. In response to simple mechanical steps, the neuron responds to stimulus onset and offset, that is, to displacement changes or velocity (**Figure S1a**). Using gaussian white noise stimuli, we found that stimulus velocity is encoded into spike burst duration. Bursts were identified in the recordings using the distribution of interspike intervals (see *Supplementary text* and **Figure S1c,d**). We found that bursts are separated by at least 50ms, a value very different from the intraburst time intervals that have 10ms as their most probable value. The

distribution of velocity values before a burst of spikes peaks at a positive (entering the skin) and with lower probability at negative (exiting the skin) velocity values, (**Fig. 2a**). Compare this with the distribution before silences (intervals of velocity preceded or followed by at least 100ms with no firing), similar to the original gaussian stimulus centered at approximately zero velocity (**Fig. 2b**). There is an approximate symmetry in the velocity values that produce bursts when the skin is entering or exiting (**Fig. 2a**), and we thus consider for simplicity the absolute value of the velocity as the relevant coded variable. We carried out the same analysis for stimulus amplitudes and found no clear stimulus features responsible for bursting (**Fig. S2**). Longer bursts code for higher velocities, as seen in the velocity distribution before a burst of given size (**Fig. 2c**). The neuron responds to increasing stimulus velocity with bursts of increasing size, covering in this way the tail of the stimulus velocity distribution (**Fig. 2c, dashed line**). Distributions in **Figure 2c** were calculated using the stimulus in the time interval 25 to 5ms before the first spike in the burst for illustrative purposes, but any fixed time or time intervals in the coding region of 40 to 5ms before spiking would give similar results (*Supplementary text* and **Fig. S3**). To study the quality of bursts at discriminating values of stimulus velocity different from those corresponding to periods of no spiking, we performed an analysis based on an ideal observer paradigm (*Supplementary text* and **Fig. S4**). We found that isolated spikes are poor at this discrimination task while bursts of increasing size achieve excellent performance. A similar burst duration code has been predicted using biophysical models of cortical bursting neurons[44]. Although velocity is the more relevant variable coded by bursts, using principal component analysis (*Supplementary text* and **Figure S5**) we also found a small acceleration component (around 20% of total contribution to bursting versus 70% for the velocity component) to which neuron is also sensitive.

Once the relevant coded variables were found, we quantified the response of the neuron in terms of these variables. We examined the neural gain, or non-linear output, as a function of stimulus

velocity (see *Materials and methods*). Since we had found that burst duration is important for coding velocities, we first obtained the input/output relation for average burst size. The average burst size typically increases with stimulus velocity until a saturation value (**Fig. 2d**). Burst size provides a good characterization of the response for the relevant range of input velocities, but we also checked whether other codes, such as the spike rate, are able to describe the neural gain as a function of velocity. Indeed, the spike rate was also found to be a relevant code. Bursts make two contributions to spike rate, one corresponding to the spike rate within bursts and the other between bursts. The stimuli considered are very slow compared to intraburst times so the spike rate within bursts cannot code anything significantly different from burst duration. This leaves burst rate as the most relevant coding contribution to spike rate (**Fig. 2e**).

Burst size and burst rate adapt to stimulus variance

So far we have seen that stimulus velocity is coded in burst size and burst rate and that the effect of sodium pumps is to decrease excitability proportionally to stimulus velocity variance. How does this change in excitability affect coding? To answer this question we next studied how the distribution of velocities before different burst sizes was affected by the decrease of excitability with increasing stimulus variance. Bursts of two spikes, for example, are produced in response to different velocity intervals depending on the variance of the stimulus distribution (**Fig. 3a**). The relevant scaling parameter was found to be the standard deviation of the distribution of skin velocities. To see this we plotted the probabilities in **Figure3a** but this time for the ratio of the stimulus velocity to the standard deviation of the total velocity distribution (**Fig. 3b**). The scaled probabilities are now found to be independent of the stimulus variance. Bursts of a given size are then produced not in response to stimulus velocity but to the ratio of velocity and the standard

deviation of the velocity distribution. Similar adaptive scaling was found for other burst sizes and even for isolated spikes (**Fig. S6**).

The same scaling was also found in the input/output functions. The average burst sizes in response to stimulus velocities are different depending on the stimulus variance (**Fig. 3c**). The same burst sizes normalized by the mean burst duration are instead produced in response to the ratio of velocity and standard deviation of the stimulus velocity distribution (**Fig. 3d**). Burst rates show the same scaling relationship (**Fig. 4**). Similarly to the case of normalized burst sizes in **Figure 3c,d**, normalized burst rates for different input variances are elicited not proportionally to absolute velocity values (**Fig. 4a**), but to velocities relative to the standard deviation of the input distribution (**Fig. 4b**). Velocity is the most relevant variable coded but not the only one, so we also tested whether there was adaptational scaling for other relevant stimulus features. To do this we calculated the neural gain as a function of the two main stimulus filters obtained by principal component analysis (see *Supplementary text*). These two filters correspond to stimulus velocity and acceleration and both show a similar adaptation to variance (**Fig. S5**).

Blocking the sodium pump significantly disrupts adaptation to stimulus variance

Adaptation to statistics implies that a burst of given size is first produced in response to low velocities but in one minute to higher values. This implies a shift of the response to higher velocities, the higher the larger the stimulus variance. For a burst of three spikes, for example, the distribution of preceding velocities shows this shift to higher velocities (**Fig. S7a**). After blocking sodium pumps with strophantidin[30] there are at most six minutes of healthy firing response (see *Materials and methods*), enough time to observe neither hyperpolarization nor a shift to higher velocities (**Fig. S7b**). More importantly, there is a significant disruption of adaptive scaling in

presence of the sodium pump blocker strophantidin, shown for standard deviations σ_{vel}=1.5 (black) and 2.25 mm/s (red) (**Fig. 5**). This disruption of adaptive scaling takes place in all quantities implicated in the coding, including the distribution of velocities before bursts of two spikes (**Fig. 5a**), bursts of three or more spikes (**Fig. 5b**) and all bursts (**Fig. 5c**), as well as in the rate (**Fig. 5d**) and average burst duration (**Fig. 5e**). We tested that this disruption of adaptive scaling by strophantidin is not due to additional nonstationary effects of the drug by checking that input-output relationships were independent of the order of presentation of the stimulus distributions (**Fig. S8**). Activity induced hyperpolarization in this neuron is mainly due to the sodium pump, but to a lesser extent also to a calcium-dependent potassium conductance with values up to 5mV[30]. We therefore tested whether this potassium conductance has an influence on adaptational scaling using the specific blocker apamin, known to inhibit the calcium-dependent potassium conductance in the T neuron[45] (see *Materials and methods*). We found that in presence of apamin the membrane hyperpolarizes 4-5mV less than in controls (**Fig. S9**), but with no significant effect on adaptive scaling (**Fig. S10**).

Modeling shows sodium pump dynamics as a mechanism for adaptation to statistics

We further investigated the role of sodium pumps in adaptational scaling using a two compartment model. The model includes all known conductances for the neuron tested experimentally (**Fig. 6a**, *Materials and methods, Supplementary text* and ref. [46]). The response of the model neuron to simple protocols hyperpolarizing the membrane are similar to those in experiments (**Fig. 6b**; compare to experiment in **Fig. 1a**). The small gap seen in **Fig. 6b** is due to the recovery time of the after-hyperpolarization conductance $g_{K,Ca}$, which has a faster time scale than that of the sodium pump[30,46]. The sodium pump has effects in both coding and adaptational scaling. Without sodium pump, the neuron saturates earlier and thus does not code high velocities (**Fig. 6c** with pump, **Fig.**

6d without pump). Adaptational scaling takes place in the complete model until velocities twice the standard deviation of the stimulus (**Fig. 6c,e**), similarly to the experimental results (**Fig. 5**). The same model but without sodium pump dynamics shows no adaptive scaling in the normalized rate (**Fig. 6d,f**), similarly to the experimental results (**Fig. 5c,d**). Similarly, we tested that in burst coding there is no adaptive scaling without sodium pumps, for example in the distribution of stimulus velocities prior to bursts of two spikes (**Fig. S11**). Eliminating the other hyperpolarizing conductance, the calcium-dependent potassium current, but retaining the sodium pump did not eliminate the adaptational scaling (**Fig. S12**), again similarly to experimental results (**Fig. S10**). Sodium pumps are therefore the only responsible elements for adaptational scaling in the model. We have also used the model to test the generality of the effect and found that the hyperpolarization induced by sodium pump activity might be larger the smaller the neuron (*Supplementary text* and **Fig. S13**).

DISCUSSION

We have shown experimentally and using numerical simulations that sodium pump dynamics is a mechanism for adaptation to stimulus variance in the time scale of a minute. This result has four parts. We first dissected the coding properties of the bursting neuron. We found that standard measures like burst rates can be used as simple coding quantities. For a more detailed account of the coding, we showed that the neuron uses a burst code. Bursting has been found to be relevant in information transmission for its effect in the improvement of synaptic reliability[41], signal-to-noise ratio of neuronal responses[47] and in the detection of behaviorally important features in the stimuli[39]. Bursts could either act as unitary events or, alternatively, their structure might convey extra information. In relation to this second view, several proposals have been given for which burst parameters are responsible for coding. Spike frequency during bursts might select the postsynaptic

neurons that get excited[40]. Also, modeling studies of a general class of bursting neurons have shown that burst duration codes for stimulus slope[44]. Experimental support for a burst duration code has been found in visual cortex in which duration correlates with stimulus optimality[42]. Our experimental results fit very well with the theoretical prediction of burst duration coding slope, in our case the slope of skin displacements, the larger slope in skin displacement the longer the burst. The second part of the results consisted in showing that the rate and burst codes show adaptive scaling. This further supports the relevance of coding in burst size as its shows the flexibility needed for the changing real-world stimuli. In this way the system can detect the velocity of approaching objects with adaptive scaling allowing the detection of high velocities relative to common stimuli like water displacements. The third part showed that sodium pumps have a significant impact on adaptive scaling while the calcium-dependent potassium current does not. Finally, we modeled the neuron to further show that sodium pumps can be a general mechanism for adaptive scaling.

We expect sodium pumps to be relevant for adaptive scaling in other systems when tested with similar stimulation protocols. Favorable preparations are those in which hyperpolarization induced by sodium pump activity has already been shown[22-28]. Two systems close to the one used in this work are insect mechanoreceptors[27] and human skin receptors[28] for which protocols very similar to ours could be directly adapted. In hippocampal pyramidal neurons there is a brief hyperpolarization of 1s due to calcium-dependent potassium current and a hyperpolarization of 20mV lasting a minute that is due in normal conditions mainly to the sodium pump[24], similarly to the leech T neuron. The functional relevance of this hyperpolarization in hippocampus may be seen as a way to avoid overexcitation[25], but more generally it might scale neuronal responses to input statistics. In hippocampal neurons, when sodium pump activity is reduced, there is still hyperpolarization due to a sodium sensitive potassium conductance[24]. The situation seems to be reversed in visual cortex,

where there is hyperpolarization due to activity affecting the time scale of 30s that is mostly due to a sodium-dependent potassium current and in which sodium pumps might be secondary[19]. Generally, sodium pumps and some potassium conductances might hyperpolarize the membrane in overlapping time scales in many neurons, with differences in their relative importance, as in the T neuron, hippocampus[24,25], C-fibers in the bullfrog sciatic nerve[26], insect mechanoreceptors[27] and probably in visual cortex[19,20]. Adaptational scaling in bipolar cells in the retina has been shown to be due to slow sodium inactivation[18,21]. This is an effect that might be quite general in the time scale of a second and that is, in principle, compatible with adaptational scaling in the scale of a minute due to sodium-pump activity. Generally, adaptational scaling might have several single neuron mechanisms acting at different time scales to cope with the complex dynamics of stimuli, as well as on the same time-scale probably to cope with different constraints like allowing modulation by different molecular mechanisms.

Acknowledgements:

William Kristan is gratefully acknowledged for support in the initial stages and Mikko Juusola for lending the mechanical stimulators and the Matlab-based BIOSYST program for data adquisition. Fabrizio Gabbiani and two anonymous referees are acknowledged for critical comments. Discussions with Brian Burton, Marco Fuenlazida, Rob Harris, Simon Laughlin, Paola Lombardo and Rossana Scuri are also appreciated. Financial support from MEC (RG, GGdP), CAM-UAM (GGdP) and BIOCIENCIA-CAM (GGdP) and a CAM fellowship (SA) is also acknowledged.

Materials and methods.

Experimental Procedures

Adult leeches Hirudo medicinalis were bought from a commercial supplier, Zaug (Germany). Animals were maintained in a large tank at 18^{o}C in natural light conditions. We used semi-intact animal preparations typically consisting of 3 or 4 ganglia (G7-G9/10) with intact connections from the central ganglia to their corresponding skin flaps. We recorded from the central ganglia and used the skin of the outer segments to pin the skin flaps to a Petri dish filled with Sylgard (Dow Corning). Extracelular solution contained (mM): 115 NaCl, 4 KCl, 1.8 $CaCl_2.2H_20$, 1.5 $MgCl_2.2H_20$, 10 Glucose, 4.6 Tris Maleate, 5.4 Tris Base, adding NaOH to a pH of 7.4 at room temperature. To block sodium pumps, we bath applied strophantidin 0.15 mM in extracellular solution in a final concentration of 1% ethanol to better dissolve the drug[30]. The solution with the drug was applied first quickly exchanging control solution by the strophantidin solution using a pipette and afterwards under constant flow at 1ml/min. We tested that the drug was effective after 15 min using a stimulation protocol like the one shown in **Fig. 1(a)**. Experiments with strophantidin used white noise stimulation of 3 minutes for each standard deviation and we typically found six minutes of healthy firing. Before addition of strophantidin, a control experiment again in a final concentration of 1% ethanol was performed using the same stimulation protocol. For these short recordings we used σ_{vel} =1.5 and 2.25 mm/s because larger standard deviations are more likely to deteriorate the electrophysiology due to vibrations in the preparation and lower ones show more variability in the rescaling, especially for for short recordings. To block the calcium-dependent potassium conductance, we used the bee venom peptide apamin at 1 nM concentration, known to block this conductance in the T neuron after 15min of its application[45]. We tested its action using stimulus protocols showing approximately 5mV of reduced hyperpolarization (**Fig. S9**). We obtained 10 minutes long recordings for two stimulus standard deviations in presence of apamin.

For a fair comparison between results with apamin and strophantidin, statistical analysis was always performed in the range 0-2 of scaled velocities, above which there is less data for analysis, especially in short recordings. Microelectrodes were pulled using a laser puller (P-2000, Sutter Instruments) with inner and outer diameters 0.5 and 1mm, respectively and backfilled with 4 M KAch with a final resistance of 40-70 MΩ. Amplification was achieved with an Axoclamp 1A amplifier and data was collected using a National Instrument card and custom-made data acquisition software in MatLab kindly provided by M. Juusola. Mechanical stimulation of the skin was performed using a closed-loop mechanical stimulator[48] (see ref [49] for displacement and frequency distributions of the manipulator). Computer-aided stimulation of random displacements was done from above and approximately perpendicular to the skin using a 2.5mm plastic ball in contact with the skin. The ball was first pushed against the elastic skin to a point from which the random displacements do not detach the ball from the skin and spikes in the T cell are always produced in response to stimuli. The skin was tested to follow the movement of the ball as by increasing the stimulus velocity with the same amplitude more spikes would be elicited and still following the different patterns in the stimulus. The stimulus range has a maximum of 1mm with 0.1μm resolution and a frequency range of 0-100 Hz. Pseudorandom stimuli with Gaussian distributions of displacements and a maximum frequency of 20Hz were used.

Data Analysis

Custom Matlab software was written to analyse the experimental data in terms of distributions and input/output relations. We separated bursts in the recording with the aid of the inter-spike-interval distribution (*Supplementary text* and **Figure S1c,d**).The stimulus dependent bursting probability, $P(b \mid s)$, or bursting rate *r(s)*, was obtained from Bayes' theorem, $P(b \mid s) / P(b) = P(s \mid b) / P(s)$, where $P(s \mid b)$ is easily obtained from the recording by taking the stimulus values previous to

bursts. For long recordings, we took stimulus intervals in one of two ways. Either using 20 ms centered at t=-15 ms before the onset of bursting or 20 ms around the maximum of response, both corresponding to where the coding seems to be more significant (**Fig.S3**). Short recordings show less variability using the second method that was then used for the sttaistical analysis in strophantidin and apamin conditions and their controls. *P(s)* is the total stimulus distribution and *P(b)* the average burst rate, r_{av}. Results are shown for burst rates as detailed above, but we tested that analogous calculations for full spike rate give similar results, including adaptive scaling. The input/output relation for the average burst size shown in **Fig. 2d** and **3c,d** is obtained as $\langle b(s) \rangle = \sum_n P(b=n \mid s)\, n$, where $P(b=n \mid s)$ is the stimulus dependent probability for bursts of n spikes and is computed from Bayes' theorem as discussed above. To quantify the neuron's selectivity to stimulus velocities and the coding properties of different bursts, we used principal component analysis (PCA) and signal detection theory using the receiver- operating characteristic (ROC), respectively (*Supplementary Text* and **Figures S4** and **S6**).

Computational models of T-cell and bursting neurons

We modified a multi-compartment model developed by Cataldo *et al.*[46] for the leech T-neuron. Our model contains only two compartments, a soma and a dendrite, considered as equivalent electrical circuits (**Fig. 6a**). They consist of a membrane capacitance C=1 μF/cm^2 in parallel with two inward currents (a fast Na^+ current, I_{Na}, and a high threshold Ca^{2+} current, I_{Ca}), an outward persistent K^+ current, I_K, a leak current I_L and two currents solely regulated by intracellular Na^+ and Ca^{2+} pools: a Ca^{2+} activated K^+ current $I_{K,Ca}$ and the Na^+ pump I_{pump}. These two last currents are slow outward currents modulated by activity, and therefore responsible for different adaptation processes. The Ca^{2+} dependent K^+ current $I_{K,Ca}$ is fast[46,50] and the slower Na^+ pump is responsible for the long

refractory times after sustained activity[46] (**Fig. 6b**). The differential equations for the time dependence of the membrane voltage in soma and dendrite are

$$\begin{aligned} -C\frac{dV_s}{dt} &= I_L^s + I_{Na}^s + I_K^s + I_{Ca}^s + I_{K,Ca}^s + I_{pump}^s + g_c(V_s - V_d)/p \\ -C\frac{dV_d}{dt} &= I_L^d + I_{Na}^d + I_K^d + I_{Ca}^d + I_{K,Ca}^d + I_{pump}^d + g_c(V_d - V_s)/(1-p) - I_{stim} \end{aligned} \quad (1)$$

where the indices *s* (*d*) stand for soma (dendrite), g_c is the electrotonic coupling and *p* the ratio of soma to total membrane area. I_{stim} is a stimulation current with the same features than the mechanical stimulation delivered to real T cells: Gaussian white noise with a frequency cut-off and different standard deviations. Note, however, that due to the fact that mechano-electrical transduction processes are unknown, the amplitude and cut-off frequencies of the stimulus current are not directly comparable to those of the mechanical stimulation. Moreover, the T cell model responds with bursts only to upstrokes of the stimulus current (detects only positive slope as in ref [44]). Details about the mathematical form of the currents and model parameters can be found in the *Supplementary text*.

The authors declare no competing interests

FIGURE CAPTIONS

Figure 1. Sodium pump activity reduces membrane excitability more with increasing stimulus variance

(a) Top: Response of the receptor neuron (T cell) to a protocol consisting of 10s of a train of 40 μm and 1.5 Hz mechanical steps on the skin of the animal, followed by 20s of several sine wave patterns of amplitude 400 μm and 10Hz and then repeating the initial train of steps. Bottom: Response of same receptor neuron to same mechanical stimulation as in **(a)** but adding to the bath

the sodium pump blocker strophantidin. **(b)** Voltage response of mechanoreceptor (top) when stimulating the skin with gaussian white noise (GWN) of displacements with cut-off frequency 5 Hz and two different standard deviations (bottom). Red line: σ_{vel} = 0.75 mm/s. Blue line: σ_{vel} = 2.25 mm/s. **(c)** Decrease in membrane potential after 200s of GWN stimulation as a function of the standard deviation of stimulus velocities. **(d)** Average spike rate as a function of the standard deviation of stimulus velocities. Full circles: Average spike rate in the first second. Empty squares: Average firing rate after 10 min of stimulation. **(e,f)** Dynamics of membrane voltage and average spike rate adaptation for the stimulus ensembles in **(b)**. Red circles: σ_{vel} = 0.75 mm/s. Blue squares: σ_{vel} =2.25 mm/s. Solid lines in **(c)** and **(d)** are fittings to exponential curves $y=a(1-e^{-bx})$ and in **(e)** and **(f)** to a combination of exponential and power law growth/decay, $y=a(1-e^{-bx})+cx^d$ and $y=ae^{-bx}+cx^d$, respectively. Error bars are standard deviations calculated over five stimulus repetitions.

Figure 2. Coding velocity in burst size and burst rate

(a) Velocity distribution before spike bursts in response to gaussian white noise stimulus (σ_{vel} = 3 mm/s and cut-off frequency 5 Hz). **(b)** Velocity distribution before silences (intervals between bursts with at least 100 ms after/before spikes). **(c)** Velocity distributions calculated at the interval 25-5ms before bursts of different sizes. Black: Single spikes. Red: Two-spike bursts. Green: Three-spike bursts. Blue: Bursts containing four or more spikes. Dashed line is the distribution of velocities in the stimulus ensemble. **(d)** Average burst size as a function of the stimulus velocity. **(e)** Burst rate as a function of the stimulus velocity.

Figure 3. Adaptive rescaling in burst size

(a) Velocity distributions before bursts of two spikes for different stimulus ensembles. Black line: σ_{vel}=0.75. Red: σ_{vel}=1.5. Green: σ_{vel}=2.25. Orange: σ_{vel}=3. Blue: σ_{vel}=4.5 (mm/s). **(b)** Same as **(a)** but dividing velocity by σ_{vel}. **(c)** Average burst size as a function of stimulus velocity normalized by the mean burst size value at each stimulus standard deviation. Stimulus ensembles and colors as in **(a)** and **(b)**. **(d)** Average burst size as a function of the stimulus velocity rescaled by the standard deviation of the distributions.

Figure 4. Adaptive rescaling in burst rates

(a) Burst rate as a function of the stimulus velocity normalized by mean burst rate for different stimulus ensembles. Black line: σ_{vel}=0.75. Red: σ_{vel}=1.5. Green: σ_{vel}=2.25. Orange: σ_{vel}=3. Blue: σ_{vel}=4.5 (mm/s). **(b)** Same as **(a)** but dividing velocity by σ_{vel}

Figure 5. Blocking sodium pumps significantly disrupts adaptive rescaling

(a) Distribution of stimulus velocities scaled by the standard deviation of the stimulus velocity prior to bursts of 2 spikes for two stimulus ensembles with σ_{vel}=1.5 (black line) and 2.25 mm/s (red line). Control experiments show adaptive scaling (top) while in presence of the sodium pump blocker strophantidin (middle) the scaling is disrupted. As a measure of disruption of adaptive scaling, the difference in the mean value for the two ensembles, *d*, is shown to be significantly larger in the presence of strophantidin (bottom). **(b)** Same as **(a)** but for bursts of 3 or more spikes. **(c)** Same as **(a)** but for all bursts. **(d)** Same as **(a)** but for normalized burst rates. As a measure of disruption of adaptive scaling, we used the root-mean-square error (RMSE) between the two curves, shown to be significantly larger for the strophantidin condition. **(e)** Same as **(d)** but for the normalized average burst duration. p values obtained from pair-wise t-tests after checking for gaussianity condition

(Lilliefors and Jarque-Bera tests) of the differences between controls and strophantidin conditions. Error bars are sem.

Figure 6. Sodium pumps responsible for adaptive rescaling in a neuron model

(a) Electrical circuit for each of the two compartments (soma/dendrite) of a leech T cell neuron model. Ionic conductances include: leakage conductance (g_L), fast Na^+ conductance (g_{Na}), delayed rectifier K^+ conductance (g_K), high-threshold non-inactivating Ca^{2+} conductance (g_{Ca}), Ca^{2+}-activated K^+ conductance ($g_{K,Ca}$) and Na^+-activated pump current I_{NaPump}. **(b)** Top trace, black: neuron model response to a square wave stimulation (current step amplitude of 8 nA, period 1.2 s) triggering 1 spike per period, followed by a sine wave of amplitude 40 nA and frequency 2 Hz producing higher activity. Bottom trace, red: response of the neuron model *without* Na^+ pump. **(c)** Normalized burst rate for the model neuron in response to gaussian white noise current stimulation ensembles of different standard deviations: 4.5 nA (Black), 9 nA (Red), 18 (Blue) and frequency cut-off 8Hz. **(d)** Same as **(c)** but *without* Na^+ pump. **(e,f)** Normalized spike rates in **(c,d)** with the input velocity rescaled by the standard deviation of the input velocity ensemble.

REFERENCES

1. Barlow, H.B. & Mollon, J.D. *The Senses*. (Cambridge University Press, Cambridge, 1982).
2. Walraven, J., Enroth-Cugell, C., Hood, D.C., MacLeod, D.I.A. & Schnapf, J.L. *The control of visual sensitivity in visual perception: the neurophysiological foundations*. (Spillmann L, Werner SJ, New York ,1990).
3. Shapley, R. Retinal physiology: adapting to the changing scene. *Curr. Biol.* **7**, R421–R423 (1997).
4. Meister, M. & Berry, M.J. II, The neural code of the retina. *Neuron* **22**, 435–450 (1999).

5. Smirnakis, S.M., Berry, M.J., Warland, D.K., Bialek, W. & Meister, M. Adaptation of retinal processing to image contrast and spatial scale. *Nature* **386**, 69-73 (1997).
6. DeWeese, M. & Zador, A. Asymmetric dynamics in optimal variance adaptation. *Neural Comput.* **10**, 1179–1202 (1998).
7. Brenner, N., Bialek, W. & de Ruyter van Steveninck, R.R. Adaptive rescaling maximizes information transmission. *Neuron* **26,** 695-702 (2000).
8. Fairhall, A.L., Lewen, G., Bialek, W. & de Ruyter van Steveninck, R.R. Eficiency and ambiguity in an adaptive neural code. *Nature* **412**, 787-792 (2001).
9. Maravall, M., Petersen, R.S., Fairhall, A.L., Arabzadeh, E. & Diamond, M.E. Shifts in coding properties and maintenance of information transmission during adaptation in barrel cortex. *PLoS Biology* **5**, No. 2, e19 (2007)
10. Kvale, M.N. & Schreiner, C.E. Adaptation of auditory receptive fields to dynamic stimuli. *J. Neurophysiol*. **91**, 604-612 (2004).
11. Sharpee, T.O. *et al.* Adaptive filtering enhances information transmission in the visual cortex. *Nature* **439**, 936-942 (2006).
12. Abbott, L.F., Sen, K., Varela, J.A. & Nelson, S.B. Synaptic depression and cortical gain control. *Science* **275**, 220-222 (1997).
13. Tsodyks, M.V. & Markram, H. The neural code between neocortical pyramidal neurons depends on neurotransmitter release probability. *Proc. Natl. Acad. Sci. USA* **94**, 719-723 (1997).
14. Markram, H., Wang, Y. & Tsodyks, M. Differential signaling via the same axon from neocortical layer 5 pyramidal neurons. *Proc. Natl. Acad. Sci. USA* **95**, 5323-5328 (1998).
15. Stemmler, M. & Koch, C. How voltage-dependent conductances can adapt to maximize the information encoded by neuronal firing rate. *Nat. Neurosci.* **2**, 521-527 (1999).

16. Fairhall, A. & Bialek, W. Adaptive spike coding. In: *The Handbook of Brain Theory and Neural Networks*, Second Edition , 90-94 (MIT Press, Cambridge, 2002).
17. Gilboa, G., Chen, R. & Brenner, N. History-dependent multiple-time-scale dynamics in a single-neuron model. *J. Neurosci.***25**, 6479-6489 (2005).
18. Rieke, F. Temporal contrast adaptation in salamander bipolar cells. *J. Neurosci.* **21**, 9445–9454 (2001).
19. Sanchez-Vives, M.V., Nowak, L.G. & McCormick, D.A. Cellular mechanisms of long-lasting adaptation in visual cortical neurons in vitro. *J.Neurosci.* **20**, 4286-4299 (2000a).
20. Sanchez-Vives, M.V., Nowak, L.G. & McCormick, D.A. Membrane mechanisms underlying contrast adaptation in cat area 17 in vivo. *J. Neurosci.* **20**, 4267-4285 (2000b).
21. Kim, K.J. & Rieke, F. Slow Na+ inactivation and variance adaptation in salamander retinal ganglion cells. *J. Neurosci.* **23**, 1506-1516 (2003).
22. Shen, K.Z. & Johnson, S.W. Sodium pump evokes high density pump current in rat midbrain dopamine neurons. *J Physiol* **512**, 449–457 (1998).
23. Darbon, P., Tscherter, A., Yvon, C. & Streit, J. Role of the electrogenic Na/K pump in deinhibition-induced bursting in cultured spinal networks. *J. Neurophysiol.* **90**, 3119-3129 (2003).
24. B. Gustafsson and H. Wigstom, Hyperpolarization following long-lasting tetanus activation of pyramidal hippocampal cells, Brain Research 275, 159-163 (1983).
25. Vaillend, C., Mason, S.E., Cuttle, M.F. & Alger, B.E. Mechanisms of neuronal hyperexcitability caused by partial inhibition of Na(+)-K(+)-ATPases in the rat CA1 hippocampal region. *J. Neurophysiol.* **88**, 2963-2978 (2002).
26. Kobayashi, J., Ohta, M. and Terada, Y. Evidence for the involvement of Na+-K+ pump and K+ conductance in the posttetanic hyperpolarization of the tetrodoxin-resistant C-fibers in the islated bullfrog sciatic nerve, Neuroscience Lett. 236, 171-174 (1997)

27. French, A.S. Two components of rapid sensory adaptation in a cockroach mechanoreceptor neuron. *J. Neurophysiol*. **62**, Issue 3, 768-777 (1989).

28. Kiernan, M.C., Lin, C.S. & Burke, D. Differences in activity-dependent hyperpolarization in human sensory and motor axons. *J. Physiol.* **558**, 341–349 (2004)

29. Baylor, D.A. & Nicholls, J.G. After-effects of nerve impulses on signalling in the central nervous system of the leech. *J. Physiol.* **203(3),** 571-589 (1969).

30. Jansen, J.K. & Nicholls, J.G. Conductance changes, an electrogenic pump and the hyperpolarization of leech neurons following impulses. *J. Physiol.* **229**, 635-655 (1973)

31. Van Essen, D.C. The contribution of membrane hyperpolarization to adaptation and conduction block in sensory neurones of the leech. *J. Physiol.* **230(3)**, 509-534 (1973).

32. Scuri, R., Mozzachiodi, R., & Brunelli, M. Activity-dependent increase of the AHP amplitude in T sensory neurons of the leech. *J. Neurophysiol.* **88**, 2490–2500 (2002).

33. Scuri, R., Mozzachiodi, R. & Brunelli, M. Role for calcium signaling and arachidonic acid metabolites in the activity-dependent increase of AHP amplitude in leech T sensory neurons. *J. Neurophysiol.* 9**4(2)**, 1066-1073 (2005).

34. Mar, A. & Drapeau, P. Modulation of conduction block in leech mechanosensory neurons. *J. Neurosci.* **16**, 4335-4343 (1996).

35. Catarsi, S. & Brunelli, M. Serotonin depresses the after-hyperpolarization through the inhibition of the Na^+/K^+ ATPase in the sensory neurones of the leech. *J. Exp. Biol.* **155**, 261–273 (1991).

36. Catarsi, S., Garcia-Gil, M., Traina, G., & Brunelli, M. Seasonal variation of serotonin content and non-associative learning of swim induction in the leech *Hirudo medicinalis. J. Comp. Physiol. [A]* **167**, 469–474 (1990).

37. Schlue, WR. Effects of ouabain on intracellular ion activities of sensory neurons of the leech nervous system. J. Neurophysiol. **61**, 233-244 (1991)

38. Krahe, R. & Gabbiani, F. Burst firing in sensory systems. *Nat. Rev. Neurosci.* **5**, 13-23 (2004).

39. Gabbiani, F., Metzner, W., Wessel, R. & Koch, C. From stimulus encoding to feature extraction in weakly electric fish. *Nature* **384**, 564-567 (1996).

40. Izhikevich, E.M., Desai, N.S., Walcott, E.C. & Hoppensteadt, F.C. Bursts as a unit of neural information: selective communication via resonance. *Trends Neurosci.* 26, 161-167 (2003)

41. Lisman, J. Bursts as a unit of neural information: making unreliable synapses reliable. *T. Neurosci.* **20**, 38-43 (1997).

42. DeBusk, B.C., DeBruyn, E.J., Snider, R.K., Kabara, J.F. & Bonds, A.B. J. Stimulus-dependent modulation of spike burst length in cat striate cortical cells Neurophysiol. 78, 199-213 (1997)

43. Middlebrooks, J.C., Clock, A.E., Xu, L. & Green, D.M. A panoramic code for sound location by cortical neurons. Science 264, 842-844 (1994)

44. Kepecs, A., Wang, X.J. & Lisman, J. Bursting neurons signal input slope. J. Neurosci. **22**, 9053-9062 (2002)

45. Mozzachiodi, R., Scuri, R., Roberto, M. and Brunelli, M. Caulerpenyne, a toxin from the seawed caulerpa taxifolia, depresses afterhyperpolarization in invertebrate neurons. Neuroscience **107**, 519-526 (2001)

46. Cataldo, E. *et al.* Computational model of Touch sensory cells (T cells) of the leech: role of the afterhyperpolarization (AHP) in activity-dependent conduction failure. *J. Comp. Neurosci.* **18**, 5-24 (2005).

47. Livingstone, M.S., Freeman, D.C. & Hubel, D.H. Visual responses in V1 of freely viewing monkeys. Cold Spring Harb. Symp. Quant. Biol. **61**, 27-37 (1996)

48. Chubbuck, J.G. Small-motion biological stimulator. *APL Tech. Dig*. **5**, 18-23 (1966).

49. Juusola, M. & French, A., The efficiency of sensory information coding in mechanical receptors, *Neuron* **18**, 959-968 (1997).

50. Wang, X.J. Calcium coding and adaptive temporal computation in cortical pyramidal neurons. *J Neurophysiol.* **79**, 1549-1566 (1998).

Figures:

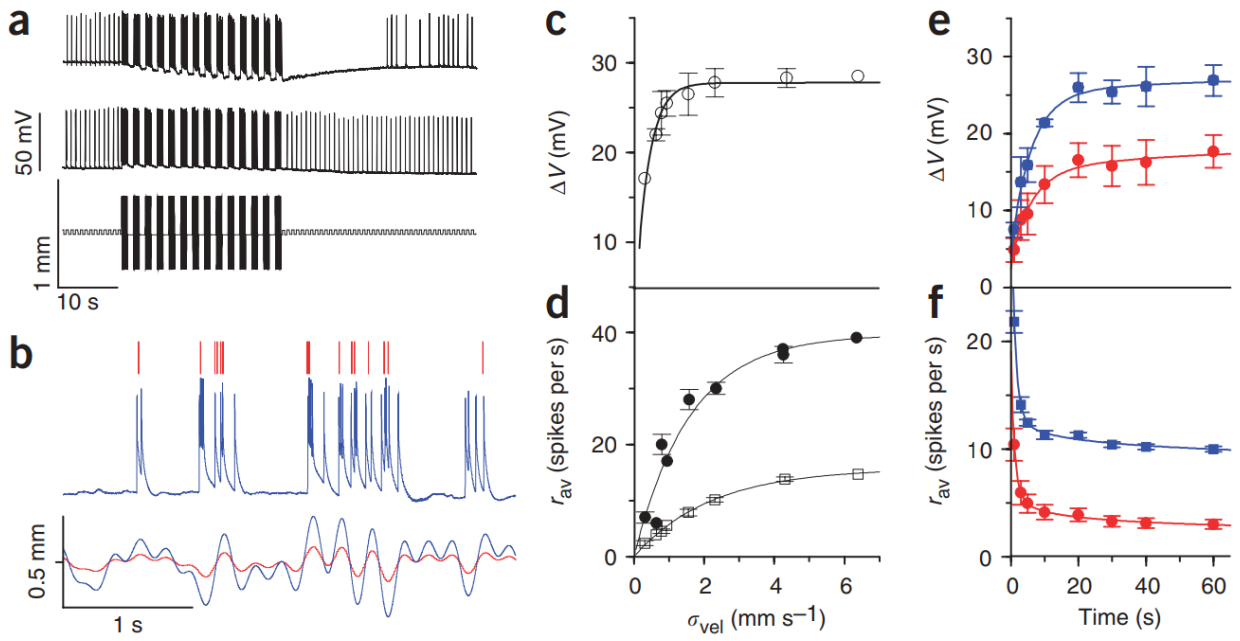

Figure 1. Reduction in membrane excitability with stimulus variance. (a) Top, response of the receptor neuron (T cell) to a protocol consisting of a 10-s train of 40-mm mechanical steps at 1.5 Hz on the skin of the leech, followed by 20 s of several 400-mm-amplitude sine-wave patterns at 10 Hz, and then repeating the initial train (bottom). Middle, response of same receptor neuron to same mechanical stimulation, but adding strophantidin to the bath solution.

(b) Voltage response of mechanoreceptor (top) when the skin was stimulated with Gaussian white noise distributions of displacements with a cutoff frequency of 5 Hz and two different s (bottom) (red line, σvel = 0.75 mm s–1; blue line, σvel = 2.25 mm s–1). (c) Decrease in membrane potential after 200 s of Gaussian white-noise stimulation as a function of σvel. (d) Average spike

rate as a function of σvel (full circles represent average spike rate in the first second; empty squares represent the average firing rate after 10 min of stimulation). Solid lines are fits to exponential curves $y = a(1 - e^{-bx})$. (e,f) Dynamics of membrane voltage and average spike rate adaptation for the stimulus ensembles in b (red circles, σvel = 0.75 mm s^{-1}; blue squares, σvel = 2.25 mm s^{-1}). Solid lines are fits to a combination of exponential and power-law growth/decay, $y = a(1 - e^{-bx}) + cx^d$ and $y = ae^{-bx} + cx^d$, respectively. Error bars are s.d.

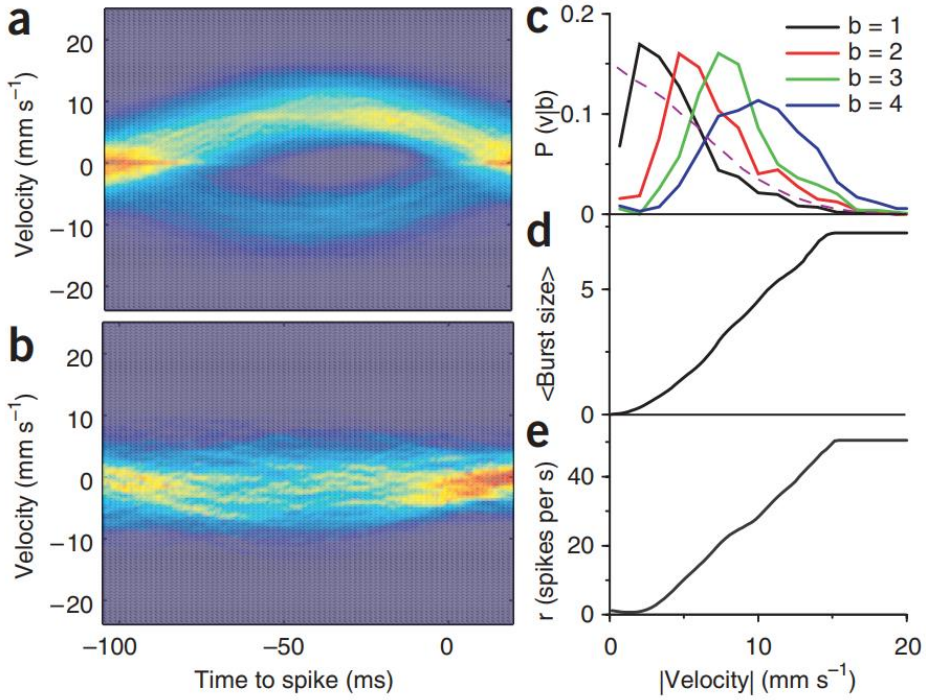

Figure 2. Burst size and rate code for mechanical velocity. (a) Velocity distribution before spike bursts in response to Gaussian white-noise stimulus (σ_{vel} = 3 mms^{-1} and cutoff frequency of 5 Hz). (b) Velocity distribution before silences (intervals between bursts with at least 100 ms after/before spikes). (c) Velocity distributions calculated at the interval 5–25 ms before bursts of different sizes (black, single spikes; red, two-spike bursts; green, three-spike bursts; blue, bursts containing four or more spikes). Dashed line is the distribution of velocities in the stimulus ensemble. (d) Average burst size as a function of the stimulus velocity. (e) Burst rate as a function of the stimulus velocity.

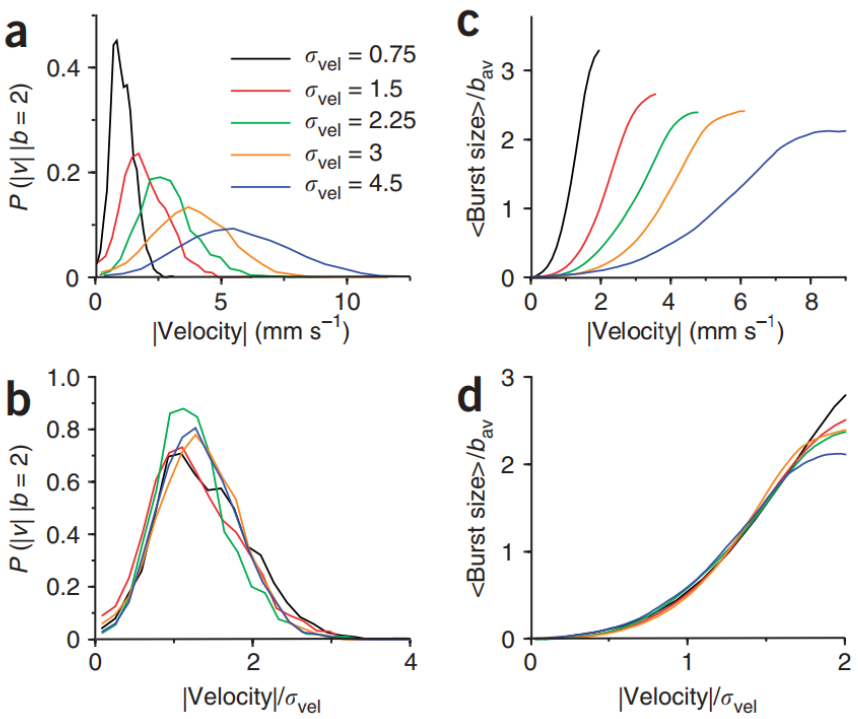

Figure 3. Adaptive rescaling in burst size. (a) Velocity distributions before bursts of two spikes for different stimulus ensembles (black line, σ_{vel} = 0.75; red, σ_{vel} = 1.5; green, σ_{vel} = 2.25; orange, σ_{vel} = 3; blue, σ_{vel} = 4.5 mm s–1). Green and blue correspond to a cutoff frequency of 10 Hz and the rest correspond to a frequency of 5 Hz. (b) Velocity distributions as in a, but with velocity divided by σ_{vel}. (c) Average burst size as a function of stimulus velocity, normalized by the mean burst-size value at each stimulus s. Stimulus ensembles and colors as in a and b. (d) Average burst size as a function of the stimulus velocity rescaled by the s of the distributions.

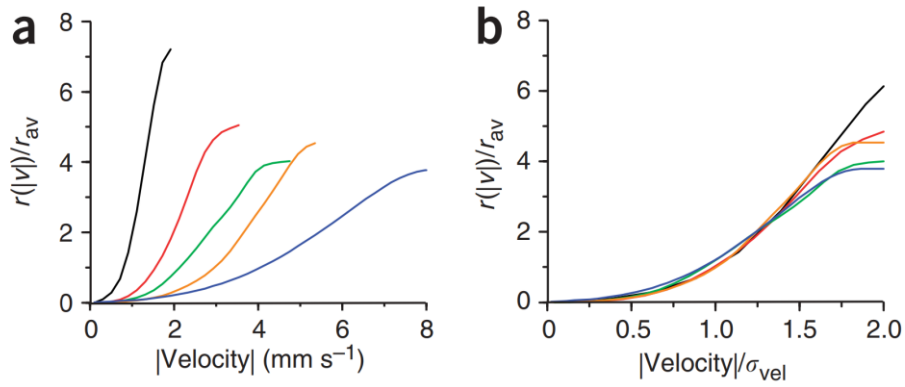

Figure 4. Adaptive rescaling in burst rates. (a) Burst rate as a function of the stimulus velocity, normalized by mean burst rate for different stimulus ensembles (black line, σ_{vel} = 0.75; red, σ_{vel} = 1.5; green, σ_{vel} = 2.25; orange, σ_{vel} = 3; blue, σ_{vel} = 4.5 mm s^{-1}). Green and blue correspond to a cutoff frequency of 10 Hz and the rest correspond to a frequency of 5 Hz. (b) Burst rate as in a, but with velocity divided by σ_{vel}

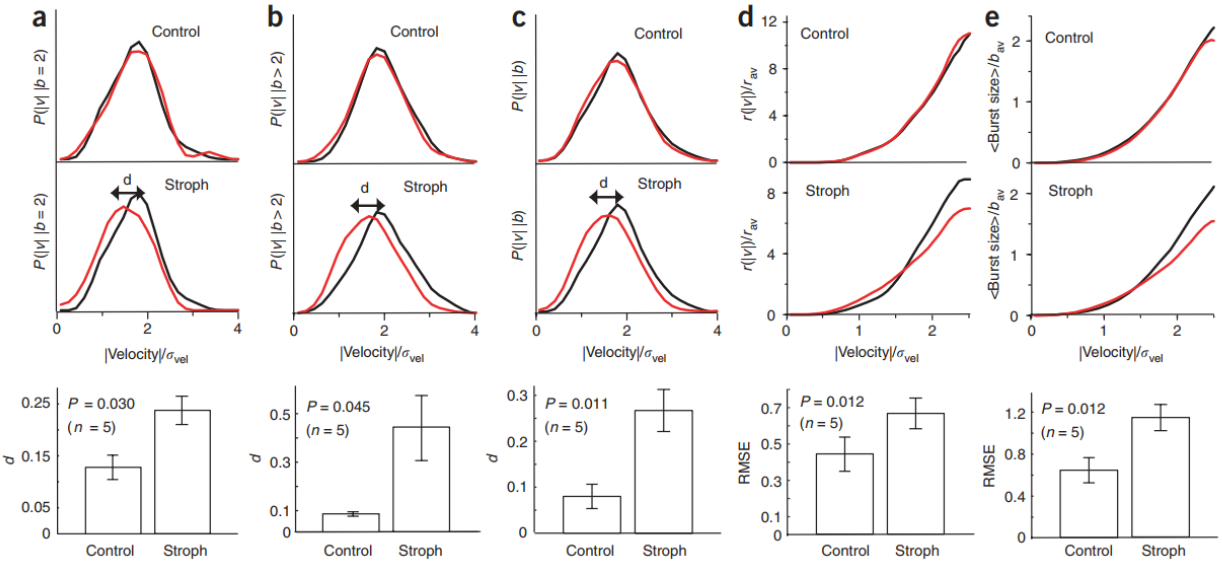

Figure 5 Blocking sodium pumps disrupts adaptive scaling. (a) Distribution of stimulus velocities scaled by the σ_{vel} before bursts of two spikes for two stimulus ensembles with σ_{vel} of 1.5 (black line) and 2.25 mm s^{-1} (red line) and a cutoff frequency of 5 Hz. Control experiments showed adaptive scaling (top), whereas the scaling was disrupted in the presence of strophantidin (middle). As a measure of disruption of adaptive scaling, the difference in the mean value of the two

ensembles, d, was significantly larger in the presence of strophantidin (bottom). (b) Distribution of stimulus velocities as in a, but for bursts of three or more spikes. (c) Distribution of stimulus velocities as in a, but for all bursts. (d) Distribution of stimulus velocities as in a, but for normalized burst rates. As a measure of disruption of adaptive scaling, we used the root-mean-square error (RMSE) between the two curves, which was significantly larger for the strophantidin condition. (e) Distribution of stimulus velocities as in d, but for the normalized average burst duration. *P* values obtained from pair-wise t-tests after checking for Gaussianity (Lilliefors and Jarque-Bera tests) of the differences between controls and strophantidin conditions. Error bars are s.e.m.